Collision of cesium atoms on helium nanodroplets: Unraveling mechanisms for surface capture at experimental velocities

David Bonhommeau

Collision of cesium atoms on helium nanodroplets: Unraveling mechanisms for surface capture at experimental velocities

David A. Bonhommeau[a)]

Université Paris-Saclay, Univ Evry, CY Cergy Paris Université, CNRS, LAMBE, Evry-Courcouronnes, 91025, France

(Dated: 23 October 2024)

The collision of cesium atoms on the surface of helium nanodroplets (HNDs) containing 1000 atoms is described by the ZPAD-mPL approach, a zero-point averaged dynamics (ZPAD) method based on a He-He pseudopotential adjusted to better reproduce the total energy of He_{1000}. Four types of collisional patterns were identified depending on the initial projectile speed v_0 and impact parameter b. At the lowest speeds ($v_0 \lesssim 250\,\mathrm{m\,s^{-1}}$) Cs atoms are softly captured by the HND surface while at the highest ones ($v_0 \gtrsim 500 - 600\,\mathrm{m\,s^{-1}}$) Cs atoms can travel through the droplet and move away. In between these two extreme cases, Cs atoms can be temporarily submerged in the HND before being expelled to the surface if $b = 0$ or cross the HND before being captured on its surface. The possibility for Cs capture at experimental velocities and droplet piercings at the highest ones contrasts with TDDFT calculations which predict Cs capture for velocities lower than $75\,\mathrm{m\,s^{-1}}$, and Ring Polymer Molecular Dynamics (RPMD) or former ZPAD-like methods which predict soft Cs capture up to $500\,\mathrm{m\,s^{-1}}$. ZPAD-mPL results are attributed to the liquid but non superfluid nature of the droplet which favors energy exchanges with the helium environment, and to low He-He binding energy and HND surface tension which can stimulate helium ejections, especially at high projectile speeds. Despite the use of a pseudopotential to model He-He interactions, the heliophobicity of Cs atoms is maintained as demonstrated by their ability to remain localized on the HND surface or to be expelled to the HND surface after transient submersion in helium.

[a)]Electronic mail: dbonhommeau@univ-evry.fr

I. INTRODUCTION

The first observation of helium droplets is attributed to H. Kamerlingh Onnes, a few months before he succeeded in liquefying helium.[1] While purifying a helium gas to prepare its subsequent free Joule expansion, he noticed the swift appearance and disappearance of a cloud of droplets. The interest for such large droplets, visible by optic means, however vanished to the advantage of helium nanodroplets (HNDs) produced by supersonic jet expansion. Due to their very low temperature, T = 0.37 K,[2,3] and superfluid nature which arises for HNDs containing more than 60 atoms,[3–5] HNDs were deemed to be the ultimate liquid matrices to perform spectroscopic studies in ultracold conditions on a wide range of atoms, molecules, clusters and polymers.[6–9]

The preliminary step of any experiment on doped HNDs is the pickup of the atomic or molecular species of interest at the surface or interior of the HND. Three decades ago, Toennies and coworkers proved the possibility for multiple capture of noble-gas atoms, H_2O and SF_6 by HNDs composed of more than one thousand atoms but their results could not pinpoint the location of the impurity.[10,11] Nowadays, most species, and in particular noble gases, are known to be heliophilic and may coagulate to form clusters or polymers within the HND. On the contrary, alkali metal atoms are heliophobic because helium-alkali interactions are highly repulsive at short range and have a shallower and longer-ranged potential well than He-He interactions. Their localization at the droplet surface then creates a dimple whose depth increases with the alkali atomic mass.[12] However, it is worth mentioning that the ionization of alkali metal atoms make them heliophilic, due to the drastic increase of the binding energy between the ion and helium atoms, and results in the formation of a helium snowball around the ion.[13–15] Moreover, alkali metal clusters located at the HND surface start being solvated in the HND when they exceed a critical size. For sodium clusters, van der Lan and coworkers detected Na_n^+ ($n \leq 20$) at electron energies just above the threshold for Penning ionization (19.8 eV) and larger ions were produced at energies just above the threshold for charge transfer (24.6 eV). They concluded that clusters with at least 21 sodium atoms should submerge in the HND because impurities inside helium are more prone to be ionized by charge transfer than Penning ionization, which is rather expected to ionize surface atoms.[16] This result was in agreement with predictions from a theoretical model based on an evaluation of the solvation and surface energy of alkali clusters.[17] Later path-integral

molecular dynamics simulations carried out on Na_nHe_N ($300 \leq N \leq 1000$) also confirmed Na_n submersion at $n \approx 20$,[18] although the size of the HND was smaller than experimental sizes ($N \approx 10^4 - 10^5$). Van der Lan and coworkers applied the same analysis to potassium clusters and identified a critical size of about 80 atoms for its submersion in HNDs.[19]

In the present paper, the collision of heliophobic cesium atoms on HNDs composed of 1000 atoms is performed at several projectile speeds and impact parameters by zero-point averaged dynamics (ZPAD). Cs atoms were preferred to lighter alkali metal atoms because the He-Cs interaction potential has a shallower well depth and larger equilibrium distance,[20] which makes Cs atoms more heliophobic than lighter alkali metal atoms and therefore more practical to investigate alkali capture on HND surfaces. The ZPAD method, which takes into account helium zero-point energy on an average manner through the use of a He-He pseudopotential, was originally devised to investigate the fragmentation dynamics of neon-doped HNDs ionized by electron impact, a highly energetic process little influenced by helium superfluidity.[21,22] Since then, several variations of ZPAD were proposed and the most recent, called ZPAD-mPL (ZPAD with modified Panzou-Lewerenz potential), proved useful to investigate the collision and coagulation of noble-gas atoms in HNDs,[23] revealing the possibility for efficient coagulation of xenon and radon atoms despite the absence of superfluidity in the model. Interestingly, results obtained for argon concurred qualitatively with more sophisticated methods, namely ring-polymer molecular dynamics (RPMD) and time-dependent density functional theory (TDDFT).[24] In particular, Ar_2 and Ar_5 clusters could be formed within the HND after the collision of an argon atom with initial speed $v_0 = 500\,\mathrm{m\,s^{-1}}$ on $ArHe_{1000}$ and Ar_4He_{1000}, respectively.

Collisions of Cs atoms on HNDs were already tackled with ZPAD at two projectile speeds ($v_0 = 50\,\mathrm{m\,s^{-1}}$ and $500\,\mathrm{m\,s^{-1}}$) but unphysical Cs rebounds off the droplet surface arose due to the excessive well depth of the He-He pseudopotential, which made the HND rather solid than liquid.[24] ZPAD-mPL corrects this shortcoming and this approach will therefore be considered here to shed some light on the mechanisms behind the capture of Cs atoms on HNDs. Moreover, while particle- and density-based methods all predict that slow Cs atoms softly deposit on the HND surface, results at $v_0 = 500\,\mathrm{m\,s^{-1}}$ diverge. Former ZPAD simulations yield Cs captures or bounces, RPMD only leads to Cs captures, and TDDFT predicts systematic HND piercing by Cs atoms. Furthermore, Cs atoms are only captured by HNDs at speeds below $75\,\mathrm{m\,s^{-1}}$ in TDDFT simulations which seems unphysical regarding

the expected speed of these atoms in the pickup chamber ($\sim 400\,\mathrm{m\,s^{-1}}$).[25] The goal of this paper is to report the different types of dynamics arising from Cs collisions on HNDs modeled by ZPAD-mPL and to show that this method can provide some clues to better comprehend the differences between former calculations using particle- and density-based approaches.

After presenting the main features of the model and relevant details of the simulations and data analysis process, ZPAD-mPL results will be compared with available TDDFT and RPMD results for Cs atoms colliding with He_{1000}. Conditions favoring the capture of Cs atoms and droplet piercing as well as limitations of the method will be discussed as a function of the projectile speed and impact parameter, and related to Cs heliophobicity in ZPAD-mPL simulations. Remarks on alkali metal collisions on HNDs and possible modeling of the submersion of alkali clusters in helium will conclude the discussion.

II. METHOD

A. Zero-point averaged dynamics

The collision of Cs atoms on HNDs composed of 1000 atoms is carried out with the ZPAD-mPL approach recently used to investigate the coagulation of noble-gas atoms inside HNDs.[23] In original ZPAD methods, atomic nuclei evolve classically on a potential-energy surface built as a sum of pairwise interaction potentials for helium atoms and impurities, where He-He interactions are described by an effective potential (or pseudopotential) including zero-point effects, He-X (X = Ne, Ar or Cs) interactions can be effective or not, and X-X interactions (if any) maintain their usual expressions.[21,22,24,26,27] ZPAD is therefore essentially equivalent to a dynamics where frozen gaussians would be centered on helium nuclei. However, convergence of He-He pseudopotentials, by an iterative procedure described in detail elsewhere,[26,28] is hard to reach because of the very diffuse nature of the helium wavefunction and the well depth of these pseudopotentials never exceeds -1.2 $\mathrm{cm^{-1}}$.[27] Despite the smallness of this value, it does not enable the HND to be liquid. The originality of the ZPAD-mPL approach is to replace the He-He pseudopotential derived iteratively for He_{1000} by a Morse potential which ensures the liquid nature of He_{1000} and a droplet total energy (-5297 K) close to the DFT prediction (-5396 K).[24] This is achieved by scaling the well depth of the Morse potential proposed by Panzou and Lewerenz to investigate the photofragmentation of I_2 molecules in

HNDs containing a few thousands atoms ($2000 \lesssim N \lesssim 9000$),[29] called the PL potential here, in such a way that the total energy of a He_{1000} cluster evolving on a potential-energy surface built as a sum of this newly scaled potential, called the modified Panzou-Lewerenz (mPL) potential, nearly equals the total energy obtained by DFT calculations. The equilibrium distance of the mPL potential is however fixed to the same value as that of the PL potential,[23] which leads to

$$V^{eff}_{He-He}(R_{ij}) = D_e\,(\,1 - \exp[-a(R_{ij} - R_e)]\,)^2 - D_e \tag{1}$$

where i and j are indices for two He atoms, $R_e = 4.1\,\text{Å}$, $D_e = 0.6\,\text{cm}^{-1}$, and $a = 1\,\text{Å}^{-1}$. The overall potential-energy surface used for ZPAD-mPL simulations of Cs collisions on He_{1000} then writes

$$V(\mathbf{R}) = \sum_{i=1}^{1000}\sum_{\substack{j=1\\j>i}}^{1000} V^{eff}_{He-He}(R_{i,j}) + \sum_{i=1}^{1000} V_{He-Cs}(R_{i,Cs}) \tag{2}$$

where $V_{He-Cs}(R)$ is the He-Cs interaction potential proposed by Patil.[20] This interaction potential is not accurate at short range and a cutoff distance $R_{cut} = 4.5\,a_0$ ($\sim 2.38\,\text{Å}$) has been imposed. At distances $R \leq R_{cut}$ the value of the interaction potential is fixed to $V_{He-Cs}(R_{cut}) \approx 0.28\,\text{eV}$. This choice has no influence on the results since the repulsive part of the potential below R_{cut} is not expected to be explored during the dynamics. Furthermore, no He-Cs effective potential has been devised because Cs atoms are heliophobic and the process to build He-X pseudopotentials assumes a spherical helium environment around the impurity.

B. Cs collisions on He_{1000}

Before investigating the collisional dynamics of Cs atoms on He_{1000}, the HND must be equilibrated at about 0.37 K. A He_{1000} structure equilibrated at 0.37 K with another He-He pseudopotential built iteratively to study the fragmentation of Ar_nHe_{1000} (n = 3, 5) upon electron bombardment[27] is used as input. The total droplet angular momentum is first fixed to zero by removing the rotational component of atomic velocities.[30] The HND is then thermostatted at $T_{ref} = 0.47\,\text{K}$, a temperature high enough to facilitate equilibration with the mPL He-He pseudopotential while preventing helium evaporation, for 100 ps by velocity rescaling with canonical sampling.[31] A constant-energy simulation is finally run for 400 ps, which enables checking for temperature maintenance throughout the dynamics. The same

process is repeated at 0.37 K which leads to a liquid He_{1000} at the typical temperature of HNDs with zero angular momentum and an average radius of 20.4 Å.

Several properties of the He_{1000} droplet modeled by ZPAD-mPL, among which its energy per helium atom, its helium density profile, and its surface tension, can be derived from the aforementioned equilibrated structure. An additional ZPAD-mPL simulation performed for 1 ns with data storage every 0.1 ps yields an energy per helium atom equal to -5.3 K, only 0.1 K above the energy predicted by DFT calculations. The density profile of He_{1000} reported in Fig. 1 for ZPAD-mPL is then obtained by convolving the radial distribution between helium atoms and the HND center of mass with the helium wave function derived from the resolution of the radial Schrödinger equation for helium atoms.[26,28] This density profile agrees more closely with DFT results than previous ZPAD-like methods do. However, the accuracy of surface tension seems to be decreased compared to previous ZPAD-like approaches.[27,29] In a previous study,[26] the surface tension of Ar_4He_{1000} has been estimated by applying a formula devised to investigate the stability of multiply charged clusters of size N,[32–34]

$$\gamma = \frac{(A + BN^{-1/3})V_{LJ}}{(36\pi)^{1/3}\sigma_{LJ}^2} \tag{3}$$

where $A = 10.3$ and $B = -2.7$ are two dimensionless constants, and van der Waals atoms or molecules are modeled as Lennard-Jones (LJ) particles with pair well depth V_{LJ} and pair diameter σ_{LJ}. Because He-He potentials are not adjusted on LJ potentials in ZPAD-like methods, the pair diameter can be either calculated from the He-He equilibrium distance according to $\sigma_1 = R_{eq}/2^{1/6}$ or replaced by the He-He pair diameter, denoted σ_2. According to Table I, surface tensions calculated from Eq.(3) and parameters specific to ZPAD-like methods always underestimate the experimental surface tension found by Iino et al. ($\gamma_{exp} = 3.536 \times 10^{-4}$ N/m)[35] and the ZPAD-mPL approach underestimates it by no less than 40%. On the surface tension point of view, the HND modeled by ZPAD-mPL therefore appears to be too liquid and Cs atoms are expected to be more prone to penetrate inside the HND upon collision than in experiments.

The equilibrated structure also serves as input to build sets of 100 input configurations for ZPAD-mPL simulations (see Fig. 2). Each set corresponds to a given initial projectile speed ($50 \text{ m s}^{-1} \leq v_0 \leq 800 \text{ m s}^{-1}$) and impact parameter b of the collision ($b = 0$ or 10 Å), b being defined as the perpendicular distance between the Cs velocity vector and the line parallel to this vector which crosses the HND center of mass. If $b = 0$, the Cs projectile is placed

at a distance of 30 Å from the HND center of mass (about 10 Å from the HND surface) along the z axis and, if $b = 10\,\text{Å}$, the Cs projectile is additionally moved by a distance b in the y-axis direction. Input configurations belonging to a given set differ from each other by the orientation of the HND, which is rotated by 36° about the x and y axes defining the median plane of the HND orthogonal to the z axis. Data were averaged over 100 trajectories because the HND is not perfectly spherical and collisions of Cs atoms on different regions of the HND surface may result in different outcomes. In particular, depositing a Cs atom with zero velocity on the HND surface yields a total energy of $-5304 \pm 6\,\text{K}$ and the solvation energy for the Cs atom is therefore $-7 \pm 6\,\text{K}$.

In all ZPAD-mPL simulations reported here, classical equations of motion are integrated with a velocity Verlet algorithm and a time step of 1 fs. Simulations were generally run for 200 ps but they may have been extended up to 20 ns when the Cs atom was submerged in the HND during the dynamics. A 200 ps trajectory is completed within a bit more than one hour on Intel Cascade Lake processors with clock speed of 2.5 GHz whereas similar RPMD and TDDFT calculations last for weeks. It is also worth noting that the time step needed to converge TDDFT calculations can significantly vary depending on the system under investigation: 1 fs for Cs collisions on He_{1000},[25] 0.1 to 0.5 fs for argon coagulation in He_{5000},[36] and 0.01 to 0.05 fs for the solvation of alkali metal ions in He_{2000}.[15] Unless otherwise specified, snapshots extracted from ZPAD-mPL simulations are depicted by assuming that the Cs projectile hits the HND from below, as illustrated in Fig. 2.

C. Trajectory analysis and fragment detection

Discriminating between mechanisms of Cs capture, bounces and droplet piercings in an automatic and unambiguous way appeared to be an involved task because of helium evaporation and possible HND fragmentation at the highest velocities considered in this study, all the more since Cs atoms are not exactly located at the HND surface but in a dimple. Low- and high-energy collisions ($v_0 \lesssim 250\,\text{m s}^{-1}$ and $v_0 \gtrsim 700\,\text{m s}^{-1}$) are generally dominated by a single type of collisional mechanism (soft Cs capture and droplet piercings, respectively, as discussed later in this manuscript) which can be confirmed by computing the distance between the Cs atom and the HND center of mass. However, at intermediate energies, several mechanisms may be involved at a given speed and impact parameter. Consequently,

collisions were analyzed by direct trajectory inspection with the VMD software[37], which also served to generate molecular pictures, and by performing a fragment analysis to determine the composition of the residual HND at the end of the dynamics. Fragments are detected by adapting an algorithm already employed to generate mass spectra within the scope of the fragmentation of multiply charged clusters[33] and the electron-impact ionization of argon-doped HNDs.[26,27] In brief, a set of first-generation fragments is defined by gathering all atoms within a sphere of radius $R_{frag} = 16$ Å (about twice as large as the He-Cs equilibrium distance) around central atoms selected in such a way that central atom $i+1$ does not belong to any of the ith first-generation fragments already defined. Higher-generation fragments are formed by merging together lower-generation fragments with atoms in common and the process is repeated until convergence of all fragments. This algorithm is expected to be little sensitive to the value of R_{frag} provided that it is applied at sufficiently long times where fragments are well defined. It allows the tracking of helium losses and the possible escape of the Cs atom, characteristic of Cs rebounds off the HND surface or HND piercings by the Cs projectile.

III. RESULTS AND DISCUSSION

A. Comparison of density- and particle-based approaches

In a recent study dedicated to the coagulation of heliophilic noble-gas atoms in HNDs, the ZPAD-mPL approach enabled us to reproduce qualitatively the results of more sophisticated RPMD and TDDFT simulations while improving the statistics of previous ZPAD simulations.[23] A similar study is conducted here where the results of ZPAD-mPL simulations at two initial Cs speeds, $v_0 = 50$ and $500\,\mathrm{m\,s^{-1}}$, and two impact parameters, $b = 0$ and 10 Å (about half the HND radius), are compared with results from RPMD, TDDFT, and former ZPAD simulations.[24,25]

At $v_0 = 50\,\mathrm{m\,s^{-1}}$, 100% of ZPAD-mPL trajectories yield soft capture of Cs atoms on the HND surface at both impact parameters, in accordance with previous RPMD and TDDFT simulations (see Fig.3a). The Cs atom is not tightly stuck to the surface but can roam on the HND surface, as illustrated in Fig.4, a behavior amplified at higher velocities and pointed out in TDDFT simulations for an impact parameter of 9 Å. On the contrary, previous ZPAD

simulations predicted 8.7% and 34.8% of Cs rebounds off the HND surface at $b = 0$ and $b = 10\,\text{Å}$, respectively, and Cs atoms localized on the HND surface seemed more static. The He-He pseudopotential considered in these simulations had a well depth of about 1.27 cm^{-1}, which made the HND rather solid and hindered surface deformations. Knowing that Cs capture on a HND is accompanied by the formation of a dimple at the HND surface,[12] a solid-like, and consequently little deformable, surface should favor bounces if the projectile velocity is insufficient to induce droplet piercing. It is worth mentioning that bounces were also observed in TDDFT simulations when $75\,\text{m}\,\text{s}^{-1} \lesssim \text{v}_0 < 200\,\text{m}\,\text{s}^{-1}$ but they were attributed to a possible underestimation of helium evaporation rates which prevented slow projectiles from dissipating efficiently their energy in helium,[25] an assumption that will be commented in more detail later in this manuscript.

At $v_0 = 500\,\text{m}\,\text{s}^{-1}$, RPMD and former ZPAD simulations mainly lead to Cs captures whereas TDDFT simulations predict that the projectile should pierce the HND and move away (see Fig.3b). ZPAD-mPL simulations exhibit intermediate behaviors. At $b = 0$, the Cs atom is fast enough to partially pierce the HND before being surrounded by helium atoms in their course of forming a spherical droplet, as depicted in the three first pictures of Fig. 5. The Cs atom is then expelled to the HND surface because of its heliophobic nature (see picture 4 of Fig. 5). Despite the non-superfluid character of the HND and the shallow well of the He-He pseudopotential (0.6 cm^{-1}) compared with the He-Cs potential well ($\sim 0.84\,\text{cm}^{-1}$), Cs heliophobicity is maintained because of the He-Cs highly repulsive wall and long-range minimum at $R_{min} = 7.73\,\text{Å}$. Indeed, the excluded volume about a submerged Cs atom can be estimated as the volume of a ball of radius R_{min}, namely 1.93 nm^3, which represents about 5.4% of the initial HND volume. In other words, 54 helium atoms should be roughly moved to submerge a Cs atom, which presumably accounts for the preferred surface localization of Cs atoms in ZPAD-mPL simulations. At $b = 10\,\text{Å}$, the Cs projectile needs to cross a smaller distance to leave the HND and complete HND piercing is achieved in two thirds of the trajectories. The last third corresponds to Cs atoms which also pierce the HND but are then too slow to escape the HND attraction, and are eventually captured. This mechanism of Cs capture is achieved within 200 ps unlike Cs submersion in helium which can extend on the nanosecond time scale. ZPAD-mPL results may seem intermediate between TDDFT and RPMD ones but we must keep in mind that Cs captures do not follow the same mechanism in ZPAD-mPL and RPMD simulations. In the latter method, the Cs

atom somewhat penetrates inside the droplet before being pushed back to the surface in a way very similar to what is observed at $v_0 \lesssim 250\,\mathrm{m\,s^{-1}}$ in ZPAD-mPL simulations.[24]

This preliminary comparison of TDDFT, RPMD, and ZPAD-like methods enlightened the ability of ZPAD-mPL to predict both Cs captures, HND piercings and unexpected transient submersions of heliophobic Cs atoms in helium, at the computational cost of classical molecular dynamics. Details on the underlying mechanisms as a function of the projectile speed and impact parameter are supplied in the next section.

B. Surface capture *vs* droplet piercing

In HND experiments, Cs atoms are expected to have velocities of a few hundreds meters per second in the pickup chamber but, surprisingly, TDDFT simulations predict that the projectile pierces the HND when $v_0 \geq 200\,\mathrm{m\,s^{-1}}$ and its sticking to the HND surface only arises when $v_0 \lesssim 50\,\mathrm{m\,s^{-1}}$.[25] Two reasons have been invoked to account for this apparent discrepancy: the possibility for Cs atoms to lose energy in the pickup chamber by traveling through several HNDs before being eventually captured and, as emphasized in the previous section, an underestimation of helium evaporation related to the mean-field description adopted in the TDDFT approach. To shed some light on this issue, ZPAD-mPL simulations have been carried out at initial Cs speeds ranging from $50\,\mathrm{m\,s^{-1}}$ to $800\,\mathrm{m\,s^{-1}}$ for 200 ps, these simulations being extended up to 20 ns when submersions in helium occurred. A fragment analysis is also performed to evaluate the average composition of the HND at the end of each simulation. Most of the subsequent results have been collected in Fig.6. The collision of Cs atoms on He_{1000} has been found to follow four patterns: (i) soft Cs capture by the HND surface, (ii) Cs submersion in helium followed by Cs expulsion to the HND surface, (iii) droplet piercing followed by Cs capture by the HND surface, and (iv) droplet piercing followed by Cs escape. For the sake of consistency with Fig.3 and to avoid multiple curves which would harm the clarity of Fig.6, all patterns which yield Cs localization on the HND surface (ie, patterns (i), (ii) if expulsion occurs, and (iii)) were cumulated under the unique label "Capture".

Soft Cs captures by the HND surface occur at low speeds, $v_0 \lesssim 250\,\mathrm{m\,s^{-1}}$, and at the two impact parameters investigated. They are characterized by very low helium evaporation rates. In our simulations, the smallest Cs@He_N droplet subject to soft Cs capture was still

composed of $\langle N \rangle \approx 998.6$ helium atoms at $t_{max} = 200\,\mathrm{ps}$ (see Fig.6b). Capture is therefore possible although less than two helium atoms have evaporated. This result contrasts with TDDFT simulations where Cs capture was indicated to be possible provided that two helium atoms evaporate,[25] which made the authors conclude that evaporation rates were presumably underestimated in their model. Due to the absence of superfluidity in ZPAD-mPL simulations, energy exchanges between liquid helium and the impurity are favored and the average temperature of helium atoms can rise up to 0.75 K, this value being reached at $b = 0$ and $v_0 = 250\,\mathrm{m\,s^{-1}}$. As illustrated in Fig. S1 of the supplementary material, the average energy per helium atom of the residual HND, excluding helium evaporation, then remains below $-4.7\,\mathrm{K}$. This result reminds TDDFT simulations carried out to model the capture of neon atoms by superfluid HNDs, where the energy per helium atom stabilizes between $-4.7\,\mathrm{K}$ and $-4.8\,\mathrm{K}$ at $t \gtrsim 50\,\mathrm{ps}$ when neon is treated classically[38] and is about -5.3 K when neon is treated quantum mechanically.[39] However, this behavior is maintained at all projectile speeds in TDDFT calculations while the energy per helium atom drastically increases in ZPAD-mPL calculations when $v_0 \gtrsim 300\,\mathrm{m\,s^{-1}}$. At $b = 0$, the kinetic energy of the projectile is mainly transferred to the HND within the first 25 ps, as inferred from the time-dependent evolution of the Cs speed reported in Fig. 7a. This energy is then distributed within the HND in such a way that helium evaporation remains negligible. At $v_0 = 250\,\mathrm{m\,s^{-1}}$, the projectile speed oscillates because the Cs atom penetrates more deeply inside the HND, which yields a local droplet deformation and some energy is given back to the impurity during its rearrangement to get a more spherical shape (see Fig.4b). However, the Cs speed at $t = 200\,\mathrm{ps}$ (ie, $\langle v \rangle \approx 8.8\,\mathrm{m\,s^{-1}}$) is only slighly higher than that obtained at $v_0 = 50\,\mathrm{m\,s^{-1}}$ (ie, $\langle v \rangle \approx 7.7\,\mathrm{m\,s^{-1}}$). It is worth mentioning that the initial increase of the projectile speed visible at $v_0 = 50\,\mathrm{m\,s^{-1}}$ in Fig.7a comes from the attraction exerted by the HND on the projectile. Indeed, the Cs atom is located at about 10 Å from the HND surface and $\sim 5\,\mathrm{ps}$ are needed for the projectile to start feeling the repulsive wall of the He-Cs interaction potential whose equilibrium distance is $R_{min} = 7.73\,\text{Å}$. Finally, trajectories run at $b = 0$ and $b = 10\,\text{Å}$ are qualitatively similar at low speeds: evaporation rates slightly increase but remain low (eg, from 0.27 to 1.05 helium atom at $v_0 = 200\,\mathrm{m\,s^{-1}}$), the projectile speed at $v_0 = 50\,\mathrm{m\,s^{-1}}$ rises due to the HND attraction for $\sim 8.6\,\mathrm{ps}$ instead of $\sim 5\,\mathrm{ps}$ at the beginning of the dynamics, and the stabilization of the Cs speed is delayed by 10-15 ps. These slight differencies are attributed to the off-centered initial position of the

projectile which compels the Cs atom to travel a longer distance before colliding with the HND and leads to a less efficient energy distribution after the collision, as pointed out in other contexts when studying the coagulation of noble-gas atoms in HNDs.[23]

The second collisional pattern yielding Cs localization on the HND surface is Cs expulsion, which is always preceded by a transient submersion of the Cs atom in helium and produces smaller doped HNDs due to increased helium evaporation. They arise at $b = 0$ and initial Cs speeds ranging from $300\,\mathrm{m\,s^{-1}}$ to $600\,\mathrm{m\,s^{-1}}$. Although Cs submersions in helium were never detected at non-zero impact parameters, the Cs atom is expected to be submerged in larger HNDs, with sizes closer to experimental ones (eg, $N = 10^4 - 10^5$). In the current simulations, transient submersions in helium may concern more than 80% of the trajectories at t = 200 ps and simulations have been extended up to 20 ns by increments of 3 ns to evaluate the propensity of Cs atoms to be expelled to the surface (see Fig.6a). Cs expulsions are expected to be favored by the intrinsic heliophobic nature of Cs atoms and by helium evaporation which yields droplet shrinking. Therefore, expulsions should become less probable after several tens of nanoseconds when the HND has significantly cooled down. As an example, at $v_0 = 500\,\mathrm{m\,s^{-1}}$, the average number of helium atoms in Cs@He_N drops from 960 at $t = 200\,\mathrm{ps}$ (see Fig.6b) to 863 at $t = 2\,\mathrm{ns}$ (see Fig.6d). The composition of the HND has not been plotted for times $t > 2\,\mathrm{ns}$ because only a fraction of trajectories were extended beyond 2 ns (those with persistent Cs submersion), and related averages would have been meaningless. Figs 6c reveals that most expulsions happen within the first 5 ns and only two trajectories, one at $v_0 = 300\,\mathrm{m\,s^{-1}}$ and another at $v_0 = 400\,\mathrm{m\,s^{-1}}$, maintained a Cs atom submerged in the droplet beyond 20 ns. The amount of Cs capture thus sums up to almost 100% at $b = 0$ when $v_0 \lesssim 500\,\mathrm{m\,s^{-1}}$ which confirms the possibility for Cs capture at experimental projectile speeds in ZPAD-mPL simulations. Moreover, the curves representing the Cs speed in Fig.7a flatten out at $t \approx 15 - 20\,\mathrm{ps}$. This feature is not a signature of submersions, which occur at later times, but reflects the HND destabilization due to the large hollow created by the projectile collision at the early times of the dynamics. The plateau disappears at $t \approx 25\,\mathrm{ps}$ when the HND starts rearranging about the submerged Cs atom (see for instance the first picture in Fig.5).

At higher velocities, the projectile is able to pierce entirely the HND but its capture remains possible if its output velocity is too small to make it escape the HND attraction. This situation can be encountered when $600\,\mathrm{m\,s^{-1}} \lesssim \mathrm{v_0} \lesssim 700\,\mathrm{m\,s^{-1}}$ at $b = 0$ and $300\,\mathrm{m\,s^{-1}} \lesssim$

$v_0 < 600\,\mathrm{m\,s^{-1}}$ at $b = 10\,$Å. A typical trajectory obtained at $v_0 = 600\,\mathrm{m\,s^{-1}}$ and $b = 0$ is illustrated in Fig.8: after piercing the HND, the slow Cs atom ($\langle v \rangle \lesssim 15\,\mathrm{m\,s^{-1}}$ according to Fig.7) sticks to the deformed HND produced by coagulation of helium atoms and remains at the HND surface in spite of the droplet rearrangement and helium evaporation (256 helium atoms are lost on average at $t = 2\,$ns). In some rare trajectories performed at $v_0 = 700\,\mathrm{m\,s^{-1}}$ and $b = 0$, the Cs atom was also found to stop at more than 15 Å from the HND before going backward and being captured by the HND surface (see Fig.9). When v_0 becomes too high ($v_0 \gtrsim 600\,\mathrm{m\,s^{-1}}$ at $b = 0$ and $v_0 \gtrsim 500\,\mathrm{m\,s^{-1}}$ at $b = 10\,$Å), the Cs atom can pierce the HND and escape which leads to extensive helium fragmentation. Fragments are not restricted to single helium atoms but can include helium clusters. Off-centered collisions at $b = 10\,$Å yield HNDs which contain at least 753 helium atoms whereas the largest fragment produced after collisions at $b = 0$ hardly contains 291 helium atoms, as depicted in Figs 6d and 6f. This fragmentation scheme is not reproduced in TDDFT simulations where superfluid helium droplets are transparent for the motion of Cs atoms at any initial projectile speed $v_0 \gtrsim 200\,\mathrm{m\,s^{-1}}$ and no extensive droplet fragmentation has been reported. As an example, a Cs atom with $v_0 = 200\,\mathrm{m\,s^{-1}}$ which collides with He_{1000} leaves the droplet with a speed of $64.7\,\mathrm{m\,s^{-1}}$ at $t = 200\,$ps in TDDFT simulations.[25] In ZPAD-mPL simulations, an output speed of $63.9\,\mathrm{m\,s^{-1}}$ can be obtained but for a much higher projectile speed of $700\,\mathrm{m\,s^{-1}}$, since no droplet piercing is possible below $600\,\mathrm{m\,s^{-1}}$ at zero impact parameter.

C. Comparisons with TDDFT simulations and ZPAD-mPL limitations

The significant and long-term loss of helium atoms at $v_0 \gtrsim 300\,\mathrm{m\,s^{-1}}$ in ZPAD-mPL simulations may come from the shallow He-He well depth and weak droplet surface tension. On the contrary, helium evaporation is sometimes considered to be underestimated in TDDFT simulations at low projectile speeds because of the underlying mean field approach. For heliophobic species, like neon and xenon atoms, the agreement between ZPAD-mPL and TDDFT is however better. 7 He atoms are ejected within the first 200 ps of a ZPAD-mPL simulation modeling the collision between a neon projectile ($v_0 = 707\,\mathrm{m\,s^{-1}}$) and $NeHe_{1000}$ at $b = 0$, and 8 He atoms evaporate when the collision occurs at $b = 10\,$Å. These numbers can be compared with TDDFT simulations dedicated to Ne + He_N ($N = 1000$ or 500) collisions where the neon projectile was treated quantum mechanically[39] or classically.[38] In both cases, about

11 He atoms were ejected from the HND at $t = 150 - 200\,\mathrm{ps}$ and $b = 0$ upon the collision of a slightly faster Ne projectile ($v_0 = 800\,\mathrm{m\,s^{-1}}$). For Xe + $XeHe_{1000}$ collisions, ZPAD-mPL simulations predict the ejection of 10 to 14 He atoms at t = 200 ps and $v_0 = 276\,\mathrm{m\,s^{-1}}$,[23] while 19 He atoms are found to leave the HND after 185 ps at $v_0 = 200\,\mathrm{m\,s^{-1}}$.[40] Although the collisional processes and projectile velocities tackled by ZPAD-mPL and TDDFT are not identical, the trends seem similar as well as the final physical outcome, namely the solvation of the rare-gas atom inside the droplet.

At speeds where rare-gas atoms remain embedded in the droplet, energy exchanges can occur between the wave created by the collision in TDDFT simulations and the successive rebounds of the impurity on the inner walls of the HND.[38] Quantum vortices also arise in TDDFT simulations due to the superfluid nature of helium. In particular, a ring vortex can form at $t \approx 75\,\mathrm{ps}$ after the collision of a Cs atom on He_{1000} at $v_0 = 200\,\mathrm{m\,s^{-1}}$ and disappears when the impurity leaves the HND.[25] Vortices were also found to be produced after the collision of neon atoms on He_{500} at high projectile angular angular momentum (L_{Ne} between 176.3 and 220.3 $\hbar$).[38]. The formation of capillary waves at the HND surface or vortices cannot be reproduced by ZPAD-like simulations since superfluidity is not included in these methods.

At high projectile speeds, TDDFT simulations predict that neon atoms should remain within the HND at all realistic projectile speeds ($v_0 \lesssim 1300\,\mathrm{m\,s^{-1}}$)[38,39] provided that the impact parameter is not too large, whereas xenon and Cs atoms should pierce the droplet at $v_0 \gtrsim 600\,\mathrm{m\,s^{-1}}$ and $v_0 \gtrsim 200\,\mathrm{m\,s^{-1}}$, respectively.[25,40] Interestingly, it was also observed that Xe atoms could remain stuck at the droplet surface while attempting to leave it surrounded by 22 He atoms. Although occurring in a different context, this ressembles the expulsion of Cs atoms temporarily submerged in He_{1000} when $300\,\mathrm{m\,s^{-1}} \lesssim \mathrm{v_0} \lesssim 600\,\mathrm{m\,s^{-1}}$. However, the extensive HND fragmentation at the highest projectile velocities ($v_0 > 600\,\mathrm{m\,s^{-1}}$) is presumably the result of the combined lack of superlfuidity in the model and low helium binding energies and droplet surface tension.

IV. CONCLUSION

The collision of Cs atoms on helium nanodroplets (HNDs) containing 1000 atoms has been modeled by zero-point averaged dynamics (ZPAD) by using the mPL He-He

pseudopotential.[23] At very low projectile speeds ($v_0 \lesssim 50\,\mathrm{m\,s^{-1}}$), soft capture of Cs atoms on the HND surface is obtained, in agreement with experimental expectations and results from TDDFT, RPMD and other ZPAD-like simulations. Deviations between experiments and theoretical approaches occur at higher speeds. In experiments, the capture of alkali atoms is achieved in the pickup chamber and Cs projectiles should acquire velocities of several hundreds meters per second. On the contrary, TDDFT predicts that the Cs projectile rebounds off the HND surface at $v_0 \gtrsim 75\,\mathrm{m\,s^{-1}}$ and pierces the HND beyond $200\,\mathrm{m\,s^{-1}}$.[25] On the other hand, RMPD and previous ZPAD-like simulations mainly predict soft capture at projectile speeds up to $500\,\mathrm{m\,s^{-1}}$ and HND piercings by the Cs atom were never reported.[24] The ZPAD-mPL approach provides an intermediate overall picture maybe more representative of experimental findings. It is characterized by four mechanisms: soft capture of Cs atoms at low velocities ($v_0 \lesssim 250\,\mathrm{m\,s^{-1}}$), HND piercings followed by Cs escape at the highest velocities ($v_0 \gtrsim 500 - 600\,\mathrm{m\,s^{-1}}$), and Cs capture at the HND surface preceded by Cs transient submersion in helium or HND piercing at intermediate velocities, submersion events being only detected at zero impact parameter.

The systematic piercing of the projectile in TDDFT simulations when $v_0 \gtrsim 200\,\mathrm{m\,s^{-1}}$ was attributed to underestimated helium evaporation rates in the simulations or to the possibility for multiple HND piercings in experiments. Piercings yield droplet deformation and the projectile speed can reach the Landau velocity for the density functional in use but no extensive fragmentation was reported. On the contrary, Cs capture is possible up to $v_0 = 250\,\mathrm{m\,s^{-1}}$ with very limited helium evaporation in ZPAD-mPL simulations and HND piercings can make the droplet explode into several subclusters at $v_0 \gtrsim 700\,\mathrm{m\,s^{-1}}$, a speed not considered in TDDFT calculations to the best of my knowledge. TDDFT simulations performed in larger HNDs ($N \gtrsim 10^4$) at high projectile speeds ($v_0 > 500\,\mathrm{m\,s^{-1}}$) would be needed to determine whether the droplet remains transparent to the projectile motion or can capture slow Cs atoms, and to assess the propensity for extensive fragmentation upon collision at high kinetic energies. The copious and long-term losses of helium atoms at droplet piercings observed in ZPAD-mPL simulations carried out at high initial Cs velocities may indeed come from the shallow well depth of the mPL potential and low surface tension of the droplet. Simulations on large HNDs would be all the more valuable since experimental HND sizes are often larger than those tackled in most theoretical models and that it seems more probable for a Cs atom to collide with a large HND than multiple smaller ones. Note that the

lack of superfluidity in ZPAD-mPL facilitates energy dissipation even if the HND is small, but taking into account superfluidity, at least in a phenomelogical manner, would probably become mandatory to reproduce experimental trends on large droplets. It is also worth reminding that current ZPAD-mPL simulations are unable to describe hydrodynamic effects like the formation and propagation of capillary waves within the droplet or the appearance of vortices due to the superfluid nature of liquid helium at low temperature, phenomena which are commonly tackled by TDDFT.[36,41]

In addition to the common soft-capture mechanisms occurring at low initial Cs speeds, ZPAD-mPL simulations suggest that surface capture of Cs atoms can also arise after droplet piercing. This capture process is accompanied by significant helium evaporation and a transient submersion of the Cs atom in helium before surface localization, but no experimental evidence for such a process seems to exist. Therefore, it would be instructive to perform Cs collisions on large helium droplets ($N \gg 1000$) at $v_0 \approx 500\,\mathrm{m\,s^{-1}}$ in an attempt to detect a post-ionization signal that would prove that high speed projectiles can travel within the droplet before being captured. This would however require to ionize the doped droplet before the heliophobic impurity has time to be expelled to the surface, which might not be an easy task.

Despite the use of a He-He pseudopotential which makes the He-He well depth shallower than the He-Cs one, the heliophobicity of Cs is maintained as confirmed by the expulsion to the HND surface of temporarily submerged Cs atoms and by the inability of Cs atoms moving on the HND surface to submerge in helium. However, it is not clear whether ZPAD-mPL, or other ZPAD-like methods based on alternative He-He pseudopotentials, would properly estimate the number of alkali metal atoms above which the submersion of alkali clusters occurs.[16,19] The average size of HNDs may vary from 10^4 to 10^5 in experiments on alkali-cluster submersion, since 10^3 He atoms typically evaporate for every additional alkali atom stuck to the HND surface, and critical sizes for the submersion of sodium and potassium clusters are 21 and ~ 80, respectively. On the theoretical side, HNDs containing ten thousands of He atoms could be produced by successive coalescence of smaller HNDs before investigating the ability of an alkali metal cluster to submerge in helium, which would be a valuable extension of the present work.

SUPPLEMENTARY MATERIAL

The supplementary material includes a figure representing the average HND energy per helium atom as a function of the initial Cs speed at $t = 200\,\mathrm{ps}$.

ACKNOWLEDGMENTS

Prof. Martí Pi, Prof. Manuel Barranco, Dr Florent Calvo and Dr Nadine Halberstadt are warmly acknowledged for providing me with data from previous publications and fruitful discussions. I also express my deepest gratitude to GENCI (Grand Equipement National de Calcul Intensif) and IDRIS (Institut du Développement et des Ressources en Informatique Scientifique) for the allocation of computational resources and technical support under grant n° AD010814624.

CONFLICTS OF INTEREST

The author has no conflicts of interest to declare.

DATA AVAILABILITY

The data that support the findings of this study are available from the corresponding author upon reasonable request.

REFERENCES

[1]H. K. Onnes, in *KNAW, Proceedings*, Vol. 11 (Amsterdam, 1909) pp. 168–185.

[2]J. Harms, M. Hartmann, B. Sartakov, J. P. Toennies, and A. F. Vilesov, J. Mol. Spectrosc. **185**, 204 (1997).

[3]S. Grebenev, J. P. Toennies, and A. F. Vilesov, Science **279**, 2083 (1998).

[4]P. Sindzingre, M. L. Klein, and D. M. Ceperley, Phys. Rev. Lett. **63**, 1601 (1989).

[5]M. V. Rama Krishna and K. B. Whaley, Phys. Rev. Lett. **64**, 1126 (1990).

[6]J. P. Toennies and A. F. Vilesov, Ann. Rev. Phys. Chem. **49**, 1 (1998).

[7]K. Nauta and R. E. Miller, Science **283**, 1895 (1999).

[8]K. Nauta and R. E. Miller, Science **287**, 293 (2000).

[9]M. Mudrich and F. Stienkemeier, Int. Rev. Phys. Chem. **33**, 301 (2014).

[10]A. Scheidemann, J. P. Toennies, and J. A. Northby, Phys. Rev. Lett. **64**, 1899 (1990).

[11]M. Lewerenz, B. Schilling, and J. P. Toennies, J. Chem. Phys. **102**, 8191 (1995).

[12]O. Bünermann, G. Droppelmann, A. Hernando, R. Mayol, and F. Stienkemeier, J. Phys. Chem. A **111**, 12684 (2007).

[13]M. Buzzacchi, D. E. Galli, and L. Reatto, Phys. Rev. B **64**, 094512 (2001).

[14]S. Müller, M. Mudrich, and F. Stienkemeier, J. Chem. Phys. **131**, 044319 (2009).

[15]E. García-Alfonso, M. Barranco, N. Halberstadt, and M. Pi, J. Chem. Phys. **160**, 164308 (2024).

[16]L. An der Lan, P. Bartl, C. Leidlmair, H. Schöbel, R. Jochum, S. Denifl, T. D. Märk, A. M. Ellis, and P. Scheier, J. Chem. Phys. **135**, 044309 (2011).

[17]C. Stark and V. V. Kresin, Phys. Rev. B **81**, 085401 (2010).

[18]F. Calvo, Phys. Rev. B **95**, 035429 (2017).

[19]L. An der Lan, P. Bartl, C. Leidlmair, H. Schöbel, S. Denifl, T. D. Märk, A. M. Ellis, and P. Scheier, Phys. Rev. B **85**, 115414 (2012).

[20]S. H. Patil, J. Chem. Phys. **94**, 8089 (1991).

[21]D. Bonhommeau, P. T. Lake, Jr., C. L. Quiniou, M. Lewerenz, and N. Halberstadt, J. Chem. Phys. **126**, 051104 (2007).

[22]D. Bonhommeau, M. Lewerenz, and N. Halberstadt, J. Chem. Phys. **128**, 054302 (2008).

[23]B. Fixot, E. Louaas, and D. A. Bonhommeau, J. Chem. Phys. **161**, 044307 (2024).

[24]E. García-Alfonso, M. Barranco, D. A. Bonhommeau, N. Halberstadt, M. Pi, and F. Calvo, J. Chem. Phys. **157**, 014106 (2022).

[25]A. Leal, D. Mateo, A. Hernando, M. Pi, and M. Barranco, Phys. Chem. Chem. Phys. **16**, 23206 (2014).

[26]N. Halberstadt and D. A. Bonhommeau, J. Chem. Phys. **152**, 234305 (2020).

[27]D. A. Bonhommeau, Chem. Phys. **550**, 111307 (2021).

[28]P. Slavíček, P. Jungwirth, M. Lewerenz, N. H. Nahler, M. Fárník, and U. Buck, J. Phys. Chem. A **107**, 7743 (2003).

[29]R. Panzou and M. Lewerenz, Mol. Phys. **119**, e1977862 (2021).

[30]J. Jellinek and D. H. Li, Phys. Rev. Lett. **62**, 241 (1989).

[31]G. Bussi, D. Donadio, and M. Parrinello, J. Chem. Phys. **126**, 014101 (2007).

[32]O. Echt, D. Kreisle, E. Recknagel, J. J. Saenz, R. Casero, and J. M. Soler, Phys. Rev. A **38**, 3236 (1988).

[33]D. A. Bonhommeau, J. Chem. Phys. **146**, 124314 (2017).

[34]D. A. Bonhommeau, Chem. Phys. Lett. **685**, 275 (2017).

[35]M. Iino, M. Suzuki, and A. J. Ikushima, J. Low Temp. Phys. **61**, 155 (1985).

[36]F. Coppens, F. Ancilotto, M. Barranco, N. Halberstadt, and M. Pi, Phys. Chem. Chem. Phys. **21**, 17423 (2019).

[37]W. Humphrey, J. Mol. Graph. **14**, 33 (1996).

[38]M. Blancafort-Jorquera, A. Vilà, and M. González, Phys. Chem. Chem. Phys. **20**, 29737 (2018).

[39]A. Vilà, M. González, and R. Mayol, Phys. Che. Chem. Phys. **18**, 2006 (2016).

[40]F. Coppens, A. Leal, M. Barranco, N. Halberstadt, and M. Pi, J. Low. Temp. Phys. **187**, 439 (2017).

[41]F. Ancilotto, M. Barranco, F. Coppens, J. Eloranta, N. Halberstadt, A. Hernando, D. Mateo, and M. Pi, Int. Rev. Phys. Chem. **36**, 621 (2017).

LIST OF TABLES

TABLE I. Surface tensions of He_{1000} calculated from Eq.(3) for ZPAD-like methods and pair diameters $\sigma_1 = R_{eq}/2^{1/6}$ and σ_2 (see text). Deviations from the experimental value[35] are indicated in parentheses.

Method	σ_1 (Å)	γ_1 ($\times 10^{-4}$ N/m)	σ_2 (Å)	γ_2 ($\times 10^{-4}$ N/m)
ZPAD[27]	3.91	3.38 (4.4%)	4.01	3.21 (9.3%)
ZPAD-PL[29]	3.65	2.47 (30.1%)	3.41	2.84 (19.7%)
ZPAD-mPL[23]	3.65	1.85 (47.6%)	3.41	2.13 (39.8%)

LIST OF FIGURES

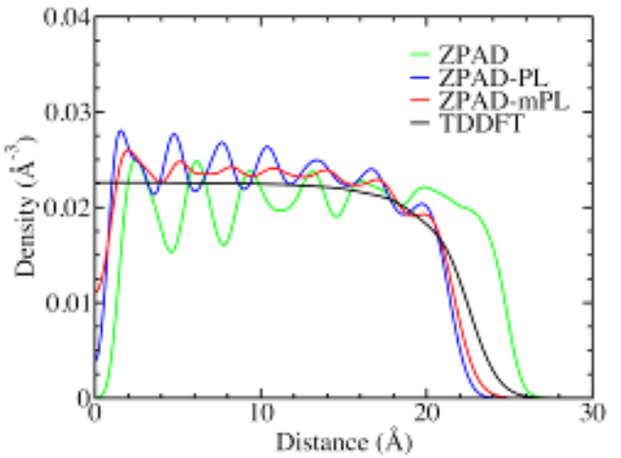

FIG. 1. Density profiles of He_{1000} after ZPAD-like and TDDFT simulations. Data for ZPAD and TDDFT methods are taken from the literature.[24,25]

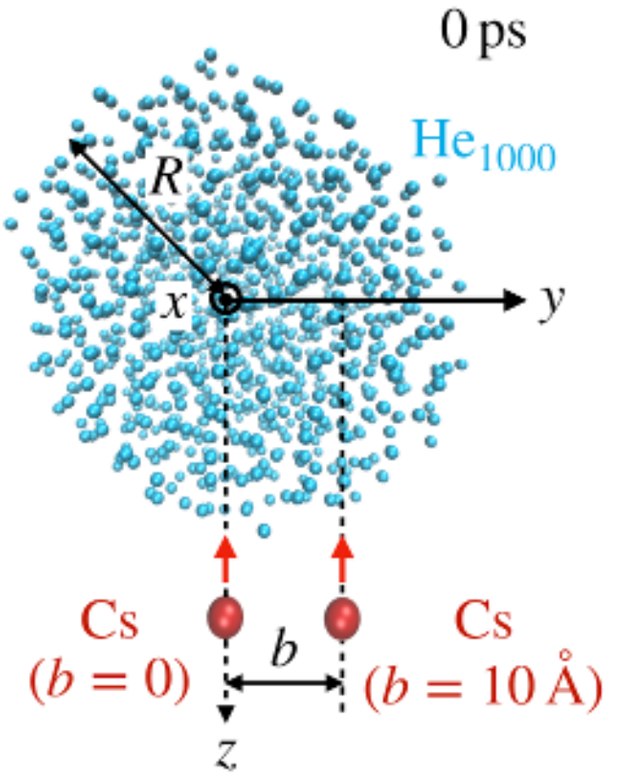

FIG. 2. Typical input configuration for Cs + He_{1000} collisions at $b = 0$ and 10 Å .

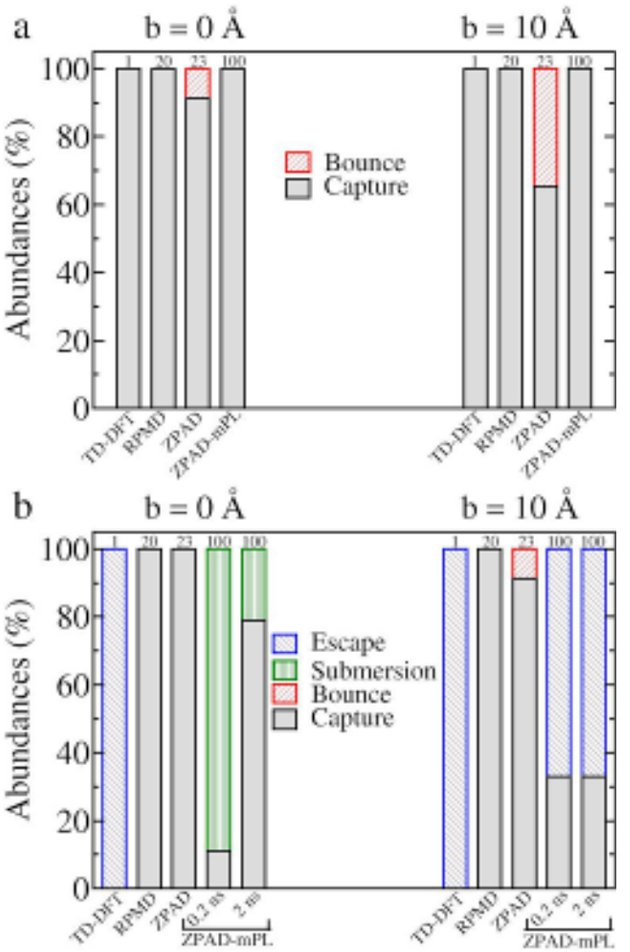

FIG. 3. Percentages of Cs atoms captured by the HND surface ("Capture"), bouncing off the HND surface ("Bounce"), submerged in the HND ("Submersion"), or moving away ("Escape") after piercing the HND, obtained by TDDFT, RPMD, and ZPAD-like simulations at Cs initial speed $v_0 = 50\,\mathrm{m\,s^{-1}}$ (a) and $v_0 = 500\,\mathrm{m\,s^{-1}}$ (b).

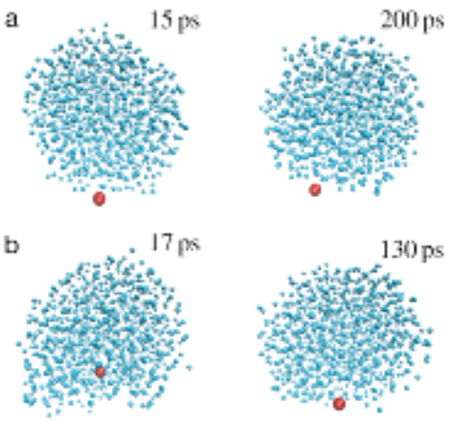

FIG. 4. Typical collision showing the soft capture on He_{1000} of a Cs atom at impact parameter $b = 0$ and initial speed $v_0 = 50\,\mathrm{m\,s^{-1}}$ (a) or $v_0 = 250\,\mathrm{m\,s^{-1}}$ (b).

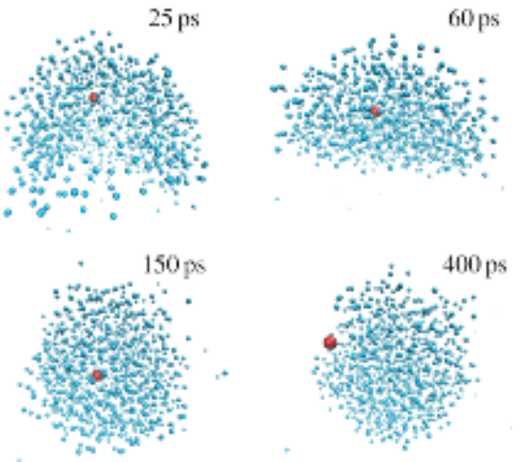

FIG. 5. Typical collision on He_{1000} of a Cs atom at impact parameter $b = 0$ and initial speed $v_0 = 500\,\mathrm{m\,s^{-1}}$. The projectile is temporarily submerged in the HND before being expelled to its surface.

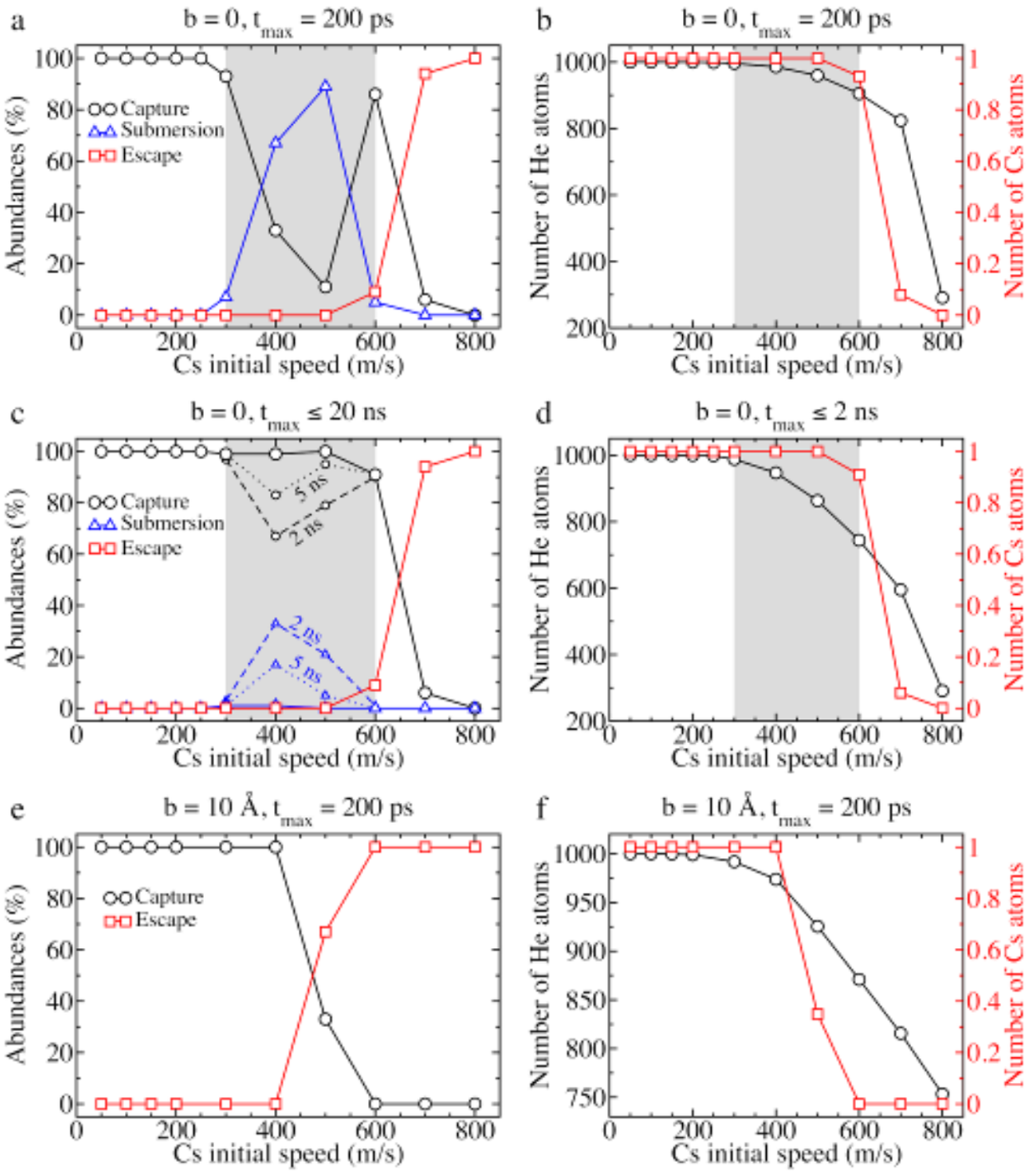

FIG. 6. Percentages of collisional processes at play during the collision of a Cs atom on He_{1000} at impact parameters $b = 0$ and 10 Å as a function of the initial projectile speed (figures a, c, and e). Captures are the sum over soft captures, expulsions after transient submersion in helium and captures after droplet piercing. The corresponding numbers of He and Cs atoms in the residual HND are depicted in the right panel (figures b, d, and f). The grey-shaded area highlights the speed interval where Cs submersions in helium occur.

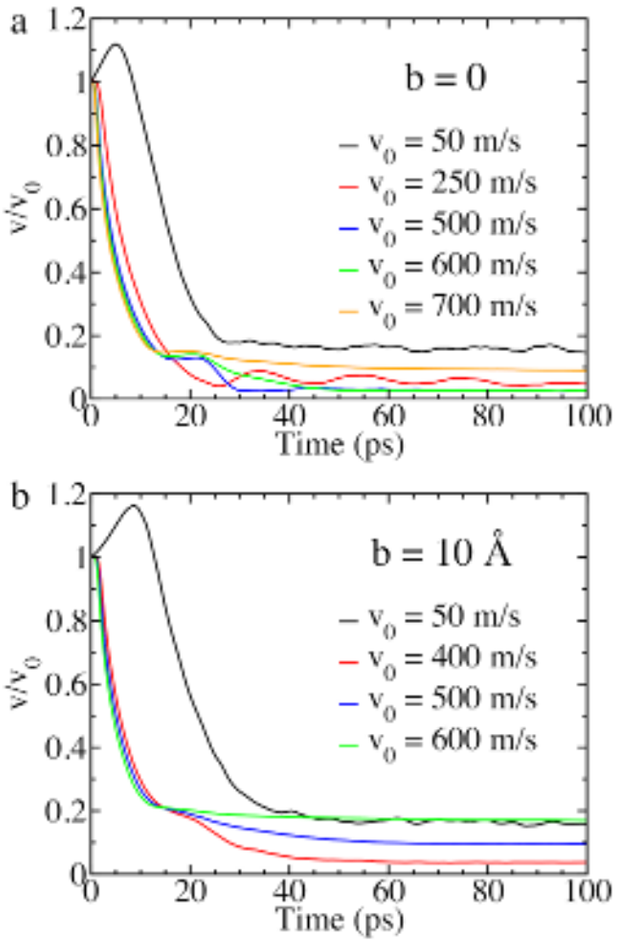

FIG. 7. Speed of Cs atoms as a function of time for $b = 0$ (a) and $b = 10$ Å (b).

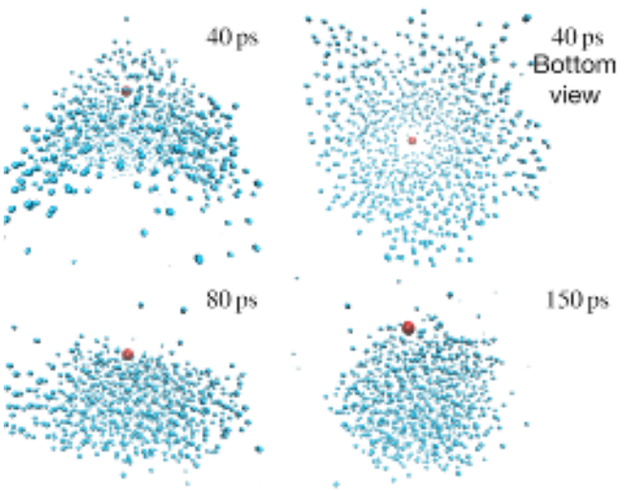

FIG. 8. Typical collision on He_{1000} of a Cs atom at impact parameter $b = 0$ and initial speed $v_0 = 600\,\mathrm{m\,s^{-1}}$. The projectile pierces the HND before being captured on its deformed surface.

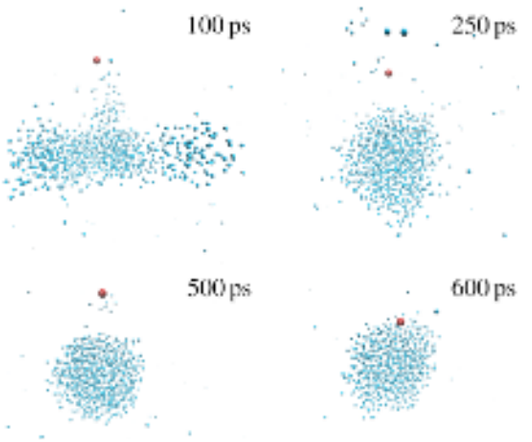

FIG. 9. Rare event showing a Cs atom at impact parameter $b = 0$ and initial speed $v_0 = 700\,\mathrm{m\,s^{-1}}$ which pierces the HND and stops in the vicinity of its surface before being captured.